INSTITUTE OF PHYSICS PUBLISHING JOURNAL OF PHYSICS B: ATOMIC, MOLECULAR AND OPTICAL PHYSICS

J. Phys. B: At. Mol. Opt. Phys. **35** (2002) 3767–3780 PII: S0953-4075(02)38130-6

Photodouble ionization differential cross sections for D_2 with various electron energy sharing conditions

D P Seccombe[1], S A Collins[1], T J Reddish[1], P Selles[2], L Malegat[2], A K Kazansky[3] and A Huetz[2]

[1] Physics Department, Newcastle University, Newcastle upon Tyne NE1 7RU, UK
[2] Laboratoire d'Interaction du Rayonnement X avec la Matière (UMR 8624), Université Paris-Sud Bâtiment 350, 91405 Orsay Cedex, France
[3] Fock Institute of Physics, The University of St Petersburg, St Petersburg, 198504, Russia

Received 13 June 2002, in final form 19 July 2002
Published 23 August 2002
Online at stacks.iop.org/JPhysB/35/3767

Abstract
The mutual angular distributions of the two ejected electrons following direct photodouble ionization have been measured for D_2 at an excess energy (E) of 25 eV using linearly polarized light. These (γ, 2e) 'triple' differential cross sections (TDCSs) were obtained for asymmetric electron energy conditions with energy sharing ratios ($R = E_2/E_1$) of $R = 24, 11.5, 4$ and 2.57. In all cases the 'reference' electron (energy $= E_1$) was oriented along the direction of the electric field vector (ε) and detected in coincidence with a second electron (energy $= E_2$) coplanar with ε and the photon beam direction ($\boldsymbol{k}_\gamma$). For comparison, helium TDCSs were obtained for the same E and R values under nearly identical spectrometer conditions. These show very good agreement with the results of hyperspherical-$\Re$-matrix with semi-classical outgoing waves calculations, thus providing even more confidence in the D_2 TDCSs where there is as yet no accurate *ab initio* theory. The similarities and differences between the experimental results associated with the two targets are qualitatively discussed in terms of Feagin's model (Feagin J M 1998 *J. Phys. B: At. Mol. Opt. Phys.* **31** L729).

1. Introduction

Photodouble ionization (PDI) of the simplest two-electron targets provides an opportunity to investigate the dynamics of a small number of unbound charged particles interacting via the long-range Coulomb force. This process has been studied extensively in helium, i.e. $h\nu + \mathrm{He} \rightarrow \mathrm{He}^{2+} + 2\mathrm{e}^-$. Experimentally, most investigations have concentrated on measuring triple differential cross sections (TDCS or $\sigma^{(3)}$), i.e. the cross section at a given energy E in excess of the PDI threshold of 79.00 eV, for ejected electrons with defined energies (E_1, $E_2 = E - E_1$) and directions (Ω_1, Ω_2). The first measured He TDCSs were reported by Schwarzkopf *et al* (1993) at $E = 20$ eV for two equal-energy electrons. This work stimulated

many other experimental and theoretical investigations, which have recently been reviewed by Briggs and Schmidt (2000). Comprehensive summaries of the experimental studies to date, which range from $E = 0.1$ to 80 eV for a variety of energy-sharing conditions ($R = E_2/E_1$), are given in Dawson *et al* (2001) and Collins *et al* (2002) for linearly and circularly polarized light, respectively.

Progress in understanding the underlying structure of the He TDCS was made by Huetz *et al* (1991), who identified its geometrical and dynamic constituents. The geometrical factors are a consequence of the symmetry of the initial state, the optical selection rules and the polarization state of the light. The charged particle dynamics were shown to be conveniently and completely described by two complex amplitudes, a_g and a_u, which are both functions of E, R and the electrons' mutual angle. These gerade (a_g) and ungerade (a_u) amplitudes are respectively symmetric and antisymmetric upon interchange of the two electrons' energies. An advantage of the symmetrized amplitudes is that the TDCS expression simplifies considerably in two special situations. These are (a) when $E_1 = E_2$, since then a_u is necessarily zero, and (b) in the threshold region, since $a_u \to 0$ faster than a_g when $E \to 0$, as demonstrated by Huetz and Mazeau (2000). Away from threshold, measuring the TDCS for a given E as a function of R is a sensitive probe of the electron dynamics (Schwarzkopf *et al* 1994, Lablanquie *et al* 1995, Mazeau *et al* 1996).

During the last decade, a variety of numerical techniques have emerged for calculating cross sections of PDI in helium and the related electron impact on atomic hydrogen problem; these include the convergent close coupling (CCC) (Bray and Stelbovics 1992, Kheifets and Bray 1998), the time-dependent close coupling (TDCC) (Pindzola and Robicheaux 2000, Colgan *et al* 2001, Colgan and Pindzola 2002), the exterior complex scaling (ECS) (Rescigno *et al* 1999, Baertschy *et al* 2001) and the hyperspherical-$\mathfrak{R}$-matrix with semi-classical outgoing waves (H$\mathfrak{R}$M-SOW) (Malegat *et al* 2000, Selles *et al* 2002) methods. In general, there is now good agreement between various *ab initio* theories and non-absolute experiments for many—but not all—kinematic situations. Regarding absolute values of the PDI cross sections, H$\mathfrak{R}$M-SOW gives very good agreement with the available experimental data. Hence, in section 3, we rely upon this theory to put the measurements on an absolute scale.

The situation is quite different for PDI of the most fundamental two-electron molecule, H_2 [$h\nu + H_2 \to 2H^+ + 2e^-$]. In this case, the H_2^{2+} repulsive potential curve, which is purely Coulombic, has a 'vertical' double ionization threshold of 51.08 eV (D_2: 51.17 eV) at the molecular equilibrium distance $R_e = 1.4$ au. The existence of a molecular axis and the two moving ionic centres add a significant degree of complexity to the PDI dynamics and, consequently, the process is less well understood than in helium. The first experiments (Dujardin *et al* 1987, Kossmann *et al* 1989) employed ion–ion coincidence measurements to determine the total PDI cross section (σ^{++}), ion asymmetry parameters (β) and kinetic energy releases associated with the Coulomb explosion. TDCSs[4] for D_2 were first reported by Reddish *et al* (1997b) at $E = 20$ eV for two equal-energy electrons and the results were later confirmed (Scherer *et al* 1998, Wightman *et al* 1998). The patterns obtained have a distinctive two-lobe structure, very similar to that observed in He. There are significant differences too, notably, the two lobes are closer together (i.e. further away from the direction of the reference electron), indicating a greater degree of electron repulsion/correlation. This effect was quantified using a He-like model with a Gaussian form for the a_g amplitude, having a half-width of $77° \pm 3°$ compared with $91° \pm 3°$ for He at the same kinematic conditions (see, for example, Wightman *et al* (1998)). In addition to this 'narrowing of the lobes', a 'filling in' of the characteristic

[4] Strictly speaking, *quadruple* differential cross sections should be used for diatomic molecules due to the Franck–Condon energy spread of the ions (see Wightman *et al* 1998). The term 'TDCS' is used here merely for convenience.

back-to-back node was observed. Further experimental work on the PDI of D_2 includes that of Dörner *et al* (1998), who, using electron–ion coincidence measurements at $E = 6.9$ eV, obtained aligned-molecule electron angular distributions, and by Collins *et al* (2001), who recently investigated the TDCS for unequal energy sharing conditions at $E = 25$ eV. Double ionization of H_2/D_2 has also been investigated using short laser pulses (e.g. Posthumus *et al* 1999, Trump *et al* 1999, Staudte *et al* 2002).

Theoretical progress has been made over the last few years in understanding the features of the differential cross sections associated with diatomic PDI. The structure of the H_2/D_2 TDCS has been analysed using a helium-like model (Feagin 1998, Reddish and Feagin 1999). This approach enabled the observed filling in of the back-to-back node, mentioned above, to be explained in terms of differences in the geometrical factors together with experimental solid angle effects. Walter and Briggs (1999) have extended the 3C (Coulomb wave) theory for He, to 5C for H_2, and examined the differential cross sections from the oriented molecule with a fixed internuclear separation. They also identified the kinematic conditions for which interference effects, arising from the two-centre nature of the core, may be observed in the electron angular distributions. The 5C TDCSs exhibit some qualitative agreement with the experimental data in that a 'narrowing of the lobes' is predicted. In a later paper (Walter and Briggs 2000) isotope effects were investigated and the selection rules for full H_2 fragmentation determined. More generally, the molecular symmetries in two-electron excited and ionized states have been studied (Walter *et al* 2000), the selection rules for PDI of rotating linear molecules have been determined (Chandra and Sen 1999) and circular dichroism has been investigated (Reddish and Feagin 1999, Sen and Chandra 2000). However, none of the numerical *ab initio* methods mentioned above (H$\Re$M-SOW, CCC, TDCC, ECS) have been applied to the diatomic PDI problem. Yet the generalization of these methods to the dynamic situation where the nuclei can be considered as fixed during the electronic escape is feasible: the description of the motion of an electron pair is technically more cumbersome in a cylindrical field than in a central field, but it does not raise new conceptual difficulties. In contrast, an accurate description of the full four-body dynamics represents a much greater challenge.

In a recent experimental study of PDI in D_2 (Collins *et al* 2001), a dual toroidal spectrometer (Reddish *et al* 1997a) was employed to measure TDCSs at $E = 25$ eV. A 20 eV electron was detected in coincidence with a 5 eV electron fixed at four different angles ($\phi_1 = 0°$, 10°, 20° and 90°) with respect to the electric field vector in the plane *perpendicular* to the photon beam direction. Helium TDCSs, measured using identical kinematics, were also presented to establish a comparison between the observed features for the two targets. The work of Collins *et al* (2001) showed interesting differences between them, but the poor statistics did not allow for definitive conclusions. Specifically, in the D_2 $\phi_1 = 0°$ spectrum, a shallow minimum in the back-to-back lobe was observed at a mutual angle of 180°. One possible explanation for this observation is that it is the signature of the anticipated interference effects associated with two ion centres. The experimental (and theoretical) evidence was, however, inconclusive.

In this study a different spectrometer was used to investigate a larger range of energy-sharing conditions for the same fixed 25 eV excess energy in both D_2 and He. Taking the energy of the fixed (reference) electron as E_1 and the second electron as E_2, D_2 and He TDCSs have been measured for $R = 24$, 11.5, 4 and 2.57. Also presented are the corresponding He TDCSs calculated using the H$\Re$M-SOW method. In all cases the fixed electron is detected along the direction of the electric field vector, a geometry that is particularly sensitive to dynamic evolution. This paper, therefore, describes a systematic study of the variation in TDCS features with R in both D_2 and helium for a fixed excess energy. The improved statistics in this work allow us to revisit issues that arose in Collins *et al* (2001) for D_2, namely the manifestation of interference effects.

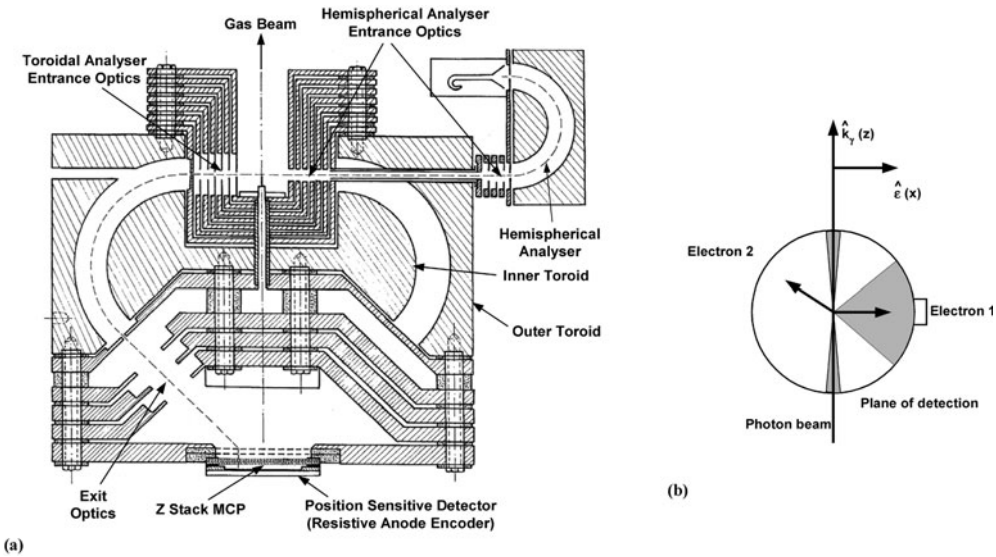

Figure 1. (a) Diagram of the spectrometer used in the present study viewed in the plane orthogonal to the photon beam direction. (b) Plan view of the detection plane showing that $\boldsymbol{k}_\gamma$, $\boldsymbol{k}_1$ and $\boldsymbol{k}_2$ are coplanar and that $\boldsymbol{k}_1$, detected by the hemispherical analyser, is aligned with the electric field vector, $\boldsymbol{\varepsilon}$. The x and z axes are in the directions of $\boldsymbol{\varepsilon}$ and $\boldsymbol{k}_\gamma$ respectively.

2. Experimental details

The present work, as with our previous study (Collins *et al* 2001), was performed using synchrotron radiation from the SU6 undulator beamline at the Super ACO storage ring. The photon beam had a polarization state described by the Stokes parameters $S_1 = 0.90 \pm 0.05$ and $S_2 = S_3 = 0$ (i.e. with a horizontal electric field direction, or a tilt angle, λ, of 0° (Dawson *et al* 2001, Collins *et al* 2001)) and an energy resolution of ≈400 meV at 75 eV. This study employed a spectrometer (Huetz *et al* 1995, Mazeau *et al* 1997) consisting of a small hemispherical analyser and a toroidal analyser fitted with a resistive anode position-sensitive detector (figure 1(a)). The incorporation of a resistive anode, available commercially from Quantar Technology, together with (custom-built) fast charge-sensitive preamplifiers and decoding electronics, improved the detection sensitivity of the spectrometer over that used in earlier work (Lablanquie *et al* 1995, Mazeau *et al* 1996). This increase in efficiency was further enhanced by the electron optical de-coupling of the entrance lens of the hemispherical analyser from that of the toroidal analyser. In this spectrometer, the electrons are detected in the plane that also contains the photon beam direction $\boldsymbol{k}_\gamma$. Within this *coplanar* geometry, the angles of emission of the electrons are given by φ_i, which varies from 0 to 360° anticlockwise from the main axis (x) of polarization $\boldsymbol{\varepsilon}$ (figure 1(b)). The electron detected by the hemispherical analyser is referred to as 'electron 1', with a direction fixed at $\varphi_1 = 0°$ and momentum vector $\boldsymbol{k}_1$; that detected by the toroidal analyser over a range of emission angles within the plane is denoted as 'electron 2' with a momentum vector $\boldsymbol{k}_2$. The angular range of the toroidal analyser is effectively reduced to 260° by three 'dead' sectors, $85° \leqslant \varphi_2 \leqslant 95°$, $265° \leqslant \varphi_2 \leqslant 275°$ and $320° \leqslant \varphi_2 \leqslant 360°/0° \leqslant \varphi_2 \leqslant 40°$, which contain the entrance and exit apertures for the photon beam, the entrance optics of the hemispherical analyser and the mechanical supports holding the inner toroid in place.

The photon energy is calibrated at the outset of the experiment, using argon, by moving the monochromator until the 6.2 eV Auger and photoelectron peaks are indistinguishable. The calibrated photon energy scale is then used to calibrate the electron energy scales of the two analysers using the $He^+(n = 2)$ peak. The energy resolutions of the two analysers (ΔE_{FWHM}) were chosen to be 500 meV. The overall coincidence resolution is 350 meV, calculated using the measured photon- and electron-energy resolutions and the appropriate equation derived in Schwarzkopf and Schmidt (1995), which takes conservation of energy into account. In D_2, the purely repulsive nature of the D_2^{2+} potential curve and the broad Franck–Condon 'overlap' distributes the PDI cross section over a large range of possible electron and ion energies. The coincidence resolution selects only a fraction of the Franck–Condon region and this, together with a relatively low total PDI cross section (σ^{++}—peak value $\sim 0.5 \times 10^{-20}$ cm^2 at $\sim$70 eV, where $\sigma^{++}/\sigma^{+} \sim$ 3–4%) results in a very low count rate. Consequently, the D_2 experiments are an order of magnitude more difficult than those using helium.

It is important that the data presented in section 3 should be scrutinized for the effects of potential systematic errors. Reflection symmetry in the measured TDCSs about the polarization axis is a necessary—but not sufficient—condition for reliability. As one can see from figure 2, the reflection symmetry is very good in most cases, implying that the correction procedure for determining the angular efficiency of the toroidal analyser is satisfactory as far as this criterion is concerned. The widely adopted correction procedure is based on measuring the He^+ ($n = 2$) photoelectron angular distribution, which is characterized by an angular asymmetry parameter, β, that has been well studied (see Wehlitz *et al* (1993) and references therein). Nevertheless, this method cannot test whether the interaction regions for single- and double-ionization experiments are identical and therefore one makes the usual assumption that the coincidence overlap is the same for all mutual angles. The observed reflection symmetry in the data supports this supposition. However, the shape of the interaction region, which is the overlap of the mutually orthogonal gas and photon beams, depends critically on the extent of the effusive gas flow, and can be elongated along the photon beam direction. Such an effect could perturb the angular distributions in the present coplanar geometry, in contrast to the perpendicular geometry which is cylindrically symmetric around the photon beam. Even so, we consider this effect, if present, to be of a relatively small magnitude as the gas inlet 'hypodermic needle' has a narrow diameter of 0.2 mm and is situated very close (<2 mm) to the centre of the detection plane. Moreover, what is ultimately important is the fraction of this potentially 'elongated' source that is imaged by the entrance optics of the hemispherical and toroidal analysers. Obviously, the fraction seen by the fixed hemispherical analyser will be constant for any given TDCS (although it may change with E_1, depending on the lens magnification). The portion viewed by the toroidal analyser, as a function of φ_2, would be the *same* for both single- and double-ionization angular distributions, and consequently corrected for by the normalization procedures. We therefore consider the potential systematic errors due to variations in the angular response to be smaller than the statistical fluctuations in the data.

The differences in the observable physics that result from the use of the *coplanar* ($\boldsymbol{k}_\gamma$, ε, $\boldsymbol{k}_1$ and $\boldsymbol{k}_2$ all lie in the same plane) and *perpendicular* ($\boldsymbol{k}_\gamma \perp \varepsilon$, $\boldsymbol{k}_1$ and $\boldsymbol{k}_2$) detection planes will be discussed in the next section.

3. Results and discussion

The helium results are discussed first so as to provide a context in which the observed features of the measured D_2 TDCSs may be interpreted. As will be seen, the united-atom limit is a suitable starting point for the description of PDI in D_2, especially at the chosen kinematic conditions.

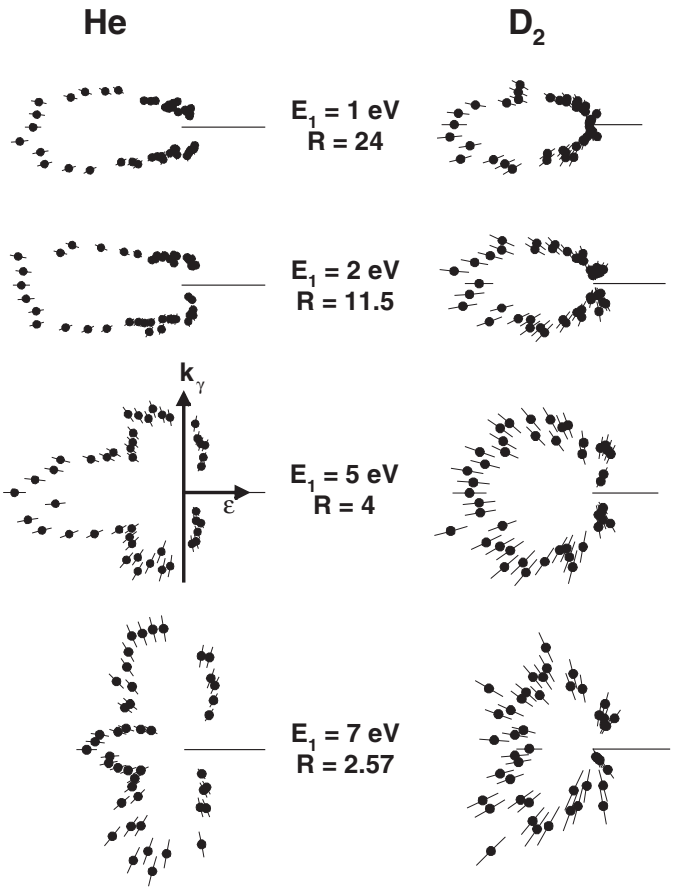

Figure 2. Comparison between the (γ, 2e) TDCSs of He and D_2 at $E = 25$ eV, $\varphi_1 = 0°$ within the coplanar detection geometry and shown in polar form.

3.1. Helium

The general structure of the TDCS, $\sigma^{(3)}$, in the case where $S_2 = S_3 = 0$, can be expressed as

$$\sigma^{(3)} = \frac{\sigma_x^{(3)} + \sigma_y^{(3)}}{2} + \frac{S_1(\sigma_x^{(3)} - \sigma_y^{(3)})}{2} \tag{1}$$

where $\sigma_x^{(3)}$ and $\sigma_y^{(3)}$ are the contributions to the TDCS arising from pure linear polarization along the x and y axes, respectively ($\boldsymbol{k}_\gamma$ lies along the z axis—see figure 1). From equation (1) it is apparent that $S_1 = +1[-1]$ corresponds to linear polarization along $x[y]$, whereas $S_1 = 0$ leads to the TDCS for unpolarized light. The general expression of the PDI TDCS for ground state helium is given by

$$\sigma^{(3)} = |a_g(\hat{\varepsilon} \cdot \hat{k}_1 + \hat{\varepsilon} \cdot \hat{k}_2) + a_u(\hat{\varepsilon} \cdot \hat{k}_1 - \hat{\varepsilon} \cdot \hat{k}_2)|^2 \tag{2}$$

where the symmetrized amplitudes a_g and a_u depend on E_1, E_2, and the mutual angle $\theta_{12} = \cos^{-1}(\hat{k}_1 \cdot \hat{k}_2)$. In the perpendicular geometry $\boldsymbol{k}_1$ and $\boldsymbol{k}_2$ lie in the xy plane and are located by their azimuthal angles ϕ_1 and ϕ_2 around the z axis (defined with respect to the x axis). For ε along the x and y axes one obtains respectively

$$\sigma_x^{(3)P} = |a_g(\cos\phi_1 + \cos\phi_2) + a_u(\cos\phi_1 - \cos\phi_2)|^2 \tag{3}$$

$$\sigma_y^{(3)P} = |a_g(\sin\phi_1 + \sin\phi_2) + a_u(\sin\phi_1 - \sin\phi_2)|^2 \tag{4}$$

and in the general case equation (1) can be used to get the TCDS in the perpendicular plane:

$$\sigma^{(3)P} = \frac{1+S_1}{2}\sigma_x^{(3)P} + \frac{1-S_1}{2}\sigma_y^{(3)P}. \tag{5}$$

In the coplanar geometry, appropriate for this study, $\boldsymbol{k}_1$ and $\boldsymbol{k}_2$ lie in the zx plane. For ε along the x and y axes, equation (2) leads to

$$\sigma_x^{(3)C} = |a_g(\cos\varphi_1 + \cos\varphi_2) + a_u(\cos\varphi_1 - \cos\varphi_2)|^2 \tag{6}$$

and to $\sigma_y^{(3)C} = 0$ as ε is then orthogonal to $\boldsymbol{k}_1$ and $\boldsymbol{k}_2$. In equation (6) φ_1 and φ_2 are now the azimuthal angles around the y axis, with zero values when $\boldsymbol{k}_1$ and $\boldsymbol{k}_2$ are along the x axis. Consequently the coplanar TDCS in the general case is given by

$$\sigma^{(3)C} = \frac{1+S_1}{2}|a_g(\cos\varphi_1 + \cos\varphi_2) + a_u(\cos\varphi_1 - \cos\varphi_2)|^2. \tag{7}$$

The principal advantage of the coplanar detection geometry is that the *shape* of the measured angular distribution is *independent* of S_1. Consequently, there is no disadvantage—in terms of interpreting the data—in not using state-of-the-art linear undulators (for which $S_1 \approx 1$). This simplification of equation (1), which only applies to the $^1S^e \rightarrow {}^1P^o$ transition, enables the contributions of a_g and a_u to the PDI dynamics to be more readily extracted from coplanar TDCSs than from perpendicular ones when $S_1 \neq 1$. It should also be noted, however, that the coplanar geometry is unsuitable for the study of circular dichroism, which becomes zero when $\boldsymbol{k}_\gamma$, $\boldsymbol{k}_1$ and $\boldsymbol{k}_2$ all lie in the same plane but is maximized in the perpendicular plane (see, for example, Berakdar and Klar (1992) and Collins *et al* (2002)).

Helium TDCSs were measured at $E = 25$ eV and $\varphi_1 = 0°$ for energies $E_1 = 1$, 2, 5 and 7 eV, corresponding to $R = 24$, 11.5, 4 and 2.57, respectively (see figure 2, column 1). The well known three-lobe structure in the angular distribution of the fast electron about the reference slow electron is evident for $R = 4$ and 2.57. The shape of the TDCS evolves with R, as expected from previous studies, and for $R = 24$ is highly peaked along the back-to-back emission direction. It is evident from equation (7) that the TDCS for $\varphi_2 = 180°$ is due purely to $|a_u|^2$, and at $\varphi_2 = 90°$ and 270° to $|a_g + a_u|^2$. Therefore, the ratio of the intensity at $\varphi_2 = 180°$ to that at $\varphi_2 = 90°$ or 270°, studied as a function of R, gives a *crude* measure of the evolution in the relative contributions of a_u and a_g, and shows the relative increase in the a_u contribution as R is increased from 2.57 to 24. This observed trend is consistent with the fact that $a_u \rightarrow 0$ as $R \rightarrow 1$. The helium TDCSs are presented in figure 3 in Cartesian form for accurate comparison with H$\Re$M-SOW calculations, displayed by the full curves. The H$\Re$M-SOW method has been described in detail elsewhere (Selles *et al* 2002) and therefore will not be discussed further here. As planned, the code has recently been transferred from a PC to a mainframe computer and this has enabled a rigorous check of the convergence of the results with respect to the size of the inner region, as well as the dimensions of the basis sets used to describe this region; this will be the subject of a forthcoming publication. The experimental TDCS plots have each been normalized to the absolute scale given by the theory in the vicinity of $\varphi_2 = 180°$. In all cases there is very good agreement between the experimental TDCSs and those obtained by the H$\Re$M-SOW calculations. Such a high level of agreement inspires even more confidence in the whole experimental procedure and in the data presented in figure 2 for both targets.

Finally, in Collins *et al* (2001), helium TDCSs were recorded at $E = 25$ eV, $R = 4$ and $\phi_1 = 0°$ with the electrons detected in the perpendicular plane. A comparison of the TDCS plot with the corresponding one from this work (see figure 2, $R = 4$) reveals a statistically

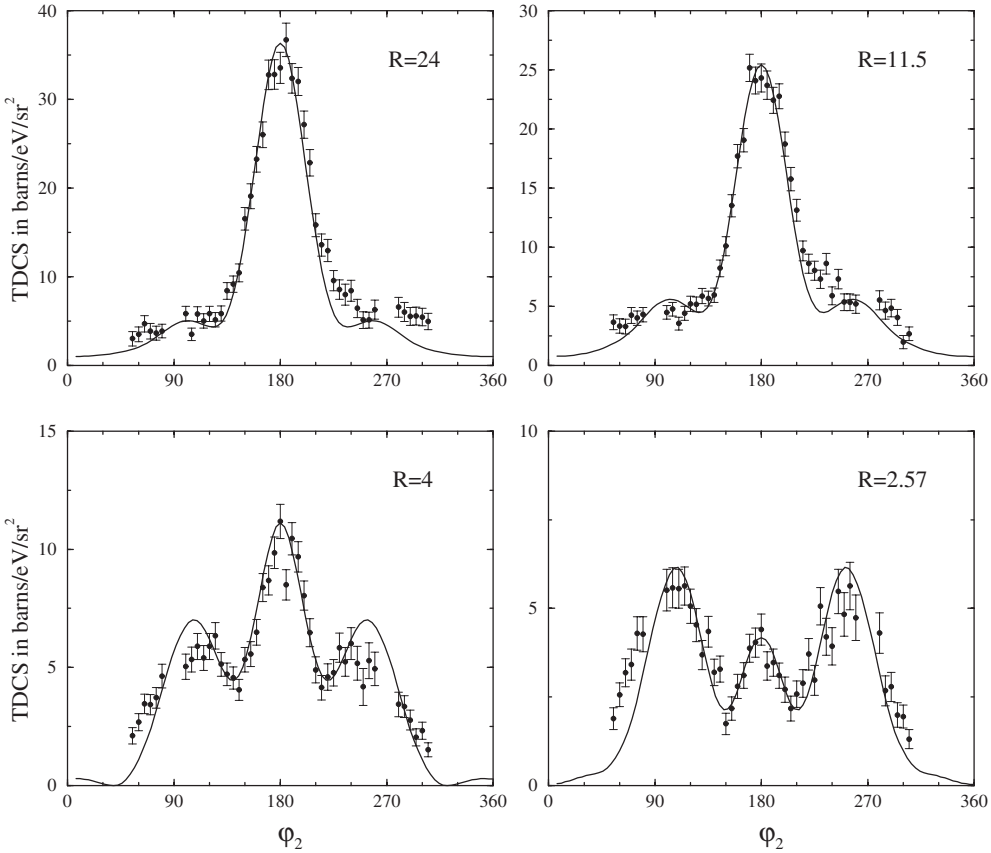

Figure 3. Comparison of the helium (γ, 2e) TDCSs measured in the present work (dots with error bars) and those computed using the H$\Im$M-SOW method (full curves).

significant difference in the ratio of the back-to-back yield to that of either 'side' lobe. The ratio in Collins *et al* (2001) was 1.0 ± 0.15, compared to 1.9 ± 0.2 here. This difference is caused in part by the two distinct detection geometries. As has been shown, $\sigma_y^{(3)P}$ is not zero (4) and, as $S_1 = 0.9 \pm 0.05$, $\sigma_y^{(3)P}$ has a finite contribution to the structure of the overall TDCS, the effect of which is to enhance the side lobes. We believe that the observed difference can also be partially explained by the lower accuracy of the previous Collins *et al* (2001) results, due to both the poorer statistics and the different method of calibrating the angular response of the analyser, the latter introducing additional uncertainties to that study.

3.2. D_2

The structure of the D_2 TDCS is somewhat more complicated than in helium. As stated in the introduction, the increase in complexity arises from the presence of a molecular axis and the two-centre nature of the 'exploding' core. The direction of the molecular axis is unknown in the present (γ, 2e) work, where only the electrons are detected. The pioneering study of Kossmann *et al* (1989) for PDI of H_2, however, has shown that the ions are preferentially emitted perpendicular to the polarization axis (negative β parameter) in the 50–100 eV photon energy range. This simple result, which has yet to receive a physical explanation, implies

that the PDI process itself partially selects a particular molecular alignment. Therefore the possible dependence of electron angular distributions on the direction of the molecular axis could influence the measured TDCS for D_2 and be partly responsible for differences with respect to helium.

Unlike helium, the angular dependence of the $D_2(\gamma, 2e)$ TDCS has not, as yet, been derived from first principles. Actually, the only available expression of the D_2 TDCS is approximate (Feagin 1998, Reddish and Feagin 1999), whereas that used above (equation (2)) for He is exact. When D_2 is doubly ionized by linearly polarized light, the polarization vector $\boldsymbol{\varepsilon}$ has components $\boldsymbol{\varepsilon}_\Sigma$ ($\boldsymbol{\varepsilon}_\Pi$) along (perpendicular to) the internuclear axis $\boldsymbol{R}$, which induce transitions from the initial Σ state to either a Σ or a Π final state. Accordingly, the PDI transition amplitude is composed of a superposition of Σ and Π contributions. Feagin's model then assumes that the angular dependence of these amplitudes, expressed in the molecular frame, is the same as in the He case. This means that (i) the $\Sigma(\Pi)$ amplitude depends only on the scalar products $\hat{k}_1 \cdot \hat{\varepsilon}_\Sigma$ and $\hat{k}_2 \cdot \hat{\varepsilon}_\Sigma$ ($\hat{k}_1 \cdot \hat{\varepsilon}_\Pi$ and $\hat{k}_2 \cdot \hat{\varepsilon}_\Pi$), and (ii) that this dependence is linear. The assumption (i) of azimuthal symmetry around each component of the polarization, valid for the Σ amplitude, clearly fails for the Π since $\boldsymbol{R} \perp \boldsymbol{\varepsilon}_\Pi$. Both (i) and (ii) correspond to postulating that the final state is dominated by the $L = 1$ partial wave, or equivalently, that the initial state of D_2 is dominated by the $L = 0$ partial wave, which is supported by the work of Joy and Parr (1958). This model, although at odds with the symmetry requirements regarding the Π amplitude, can be qualitatively helpful at low photon energies when the wavelengths of the ejected electrons are larger than the internuclear equilibrium distance R_e of the molecule. In this situation, the molecule is essentially viewed as an atom by the outgoing electron pair, so that azimuthal symmetry around the polarization component $\boldsymbol{\varepsilon}_\Pi$ is restored whatever the orientation of the molecular axis. This effect was observed by Dörner *et al* (1998) at about 7 eV above threshold when the electrons have energies less than 10 eV, i.e. $\lambda > 7$ au compared to $R_e = 1.4$ au. In the present work the highest electron energy is 24 eV and the corresponding wavelength (4.7 au) is still significantly larger than R_e. Accordingly, we shall base our discussion of the basic features of the TDCS on Feagin's model.

The following expressions of $\sigma_x^{(3)C}$ and $\sigma_y^{(3)C}$, averaged over all molecular orientations to comply with the conditions of the present experiment, are easily derived from Reddish and Feagin (1999) by resolving the Σ and Π amplitudes into their gerade (a_Σ^g, a_Π^g) and ungerade (a_Σ^u, a_Π^u) components, following the practice established for He:

$$\begin{aligned}\sigma_x^{(3)C} = {} & \tfrac{2}{15}|a_\Sigma^g(\cos\varphi_1 + \cos\varphi_2) + a_\Sigma^u(\cos\varphi_1 - \cos\varphi_2)|^2 \\ & + \tfrac{7}{15}|a_\Pi^g(\cos\varphi_1 + \cos\varphi_2) + a_\Pi^u(\cos\varphi_1 - \cos\varphi_2)|^2 \\ & + \tfrac{6}{15}\mathrm{Re}\{[a_\Sigma^g(\cos\varphi_1 + \cos\varphi_2) + a_\Sigma^u(\cos\varphi_1 - \cos\varphi_2)]^*[a_\Pi^g(\cos\varphi_1 + \cos\varphi_2) \\ & + a_\Pi^u(\cos\varphi_1 - \cos\varphi_2)]\} + \tfrac{1}{15}[|a_\alpha|^2 + |a_\beta|^2 + 2\mathrm{Re}(a_\alpha a_\beta^*)\cos(\varphi_2 - \varphi_1)] \qquad (8)\end{aligned}$$

$$\sigma_y^{(3)C} = +\tfrac{1}{15}[|a_\alpha|^2 + |a_\beta|^2 + 2\mathrm{Re}(a_\alpha a_\beta^*)\cos(\varphi_2 - \varphi_1)] \qquad (9)$$

where a_α and a_β are given by

$$a_\alpha = a_\Sigma^g - a_\Pi^g + a_\Sigma^u - a_\Pi^u \qquad (10)$$

$$a_\beta = a_\Sigma^g - a_\Pi^g - a_\Sigma^u + a_\Pi^u. \qquad (11)$$

Note that expressions for $\sigma_x^{(3)P}$ and $\sigma_y^{(3)P}$ (i.e. in the perpendicular detection plane) can *both* be obtained from equation (8) by replacing $\cos\varphi_i$ with $\cos\phi_i$ and $\sin\phi_i$, respectively (and changing $\cos(\varphi_2 - \varphi_1)$ to $\cos(\phi_2 - \phi_1)$). Unlike helium, the contribution of $\sigma_y^{(3)C}$, although reduced, is not completely eliminated in this model of D_2 PDI. $\sigma_y^{(3)C}$ depends only on the molecular PDI dynamics and on the relative azimuthal angle of the two electrons, but not on the orientation of the electric field vector. For $\sigma_y^{(3)C}$ to equal zero, a_Σ^g must equal

a^g_Π, and a^u_Σ must equal a^u_Π, which corresponds to the united atom limit. Note also that for the equal energy condition, the final term in (8), which also is equal to $\sigma_y^{(3)C}$, reduces to $4/15|a^g_\Sigma - a^g_\Pi|^2\cos^2(\theta_{12}/2)$. This results in a node in the overall TDCS for antiparallel emission as all other terms in $\sigma_x^{(3)C}$ also vanish due to their $(\cos\varphi_1 + \cos\varphi_2)$ factor.

Given the fact that all our measurements are made with $\varphi_1 = 0°$, it can be shown that at $\varphi_2 = 180°$, $\sigma_x^{(3)C,P}$ and $\sigma_y^{(3)C,P}$ reduce to

$$\sigma_x^{(3)C,P} = \tfrac{12}{15}|a^u_\Sigma|^2 + \tfrac{32}{15}|a^u_\Pi|^2 + \tfrac{16}{15}\mathrm{Re}(a^{u\,*}_\Sigma a^u_\Pi) \tag{12}$$

$$\sigma_y^{(3)C,P} = \tfrac{4}{15}|a^u_\Sigma|^2 + \tfrac{4}{15}|a^u_\Pi|^2 - \tfrac{8}{15}\mathrm{Re}(a^{u\,*}_\Sigma a^u_\Pi) \tag{13}$$

and substituting equations (12) and (13) into (1) gives

$$\sigma^{(3)C,P} = \left(\frac{1+S_1}{2}\right)\left(\frac{12}{15}|a^u_\Sigma|^2 + \frac{32}{15}|a^u_\Pi|^2 + \frac{16}{15}|a^u_\Sigma||a^u_\Pi|\cos(\delta^u_\Sigma - \delta^u_\Pi)\right) + \left(\frac{1-S_1}{2}\right)\left(\frac{4}{15}|a^u_\Sigma|^2 + \frac{4}{15}|a^u_\Pi|^2 - \frac{8}{15}|a^u_\Sigma||a^u_\Pi|\cos(\delta^u_\Sigma - \delta^u_\Pi)\right). \tag{14}$$

At this angular condition, the TDCS depends only on the two *ungerade* amplitudes and their relative phase $(\delta^u_\Sigma - \delta^u_\Pi)$; the sole dependence on the ungerade amplitudes is analogous to He, and when $a^u_\Pi = a^u_\Sigma$, equation (14) reduces to the He expression $\sigma^{(3)} = 2(1+S_1)|a_u|^2$. At other angular conditions, $\sigma^{(3)C,P}$ depends on all four amplitudes and the phase differences between each pair. Since a^u_Π and a^u_Σ are necessarily zero for the equal-energy sharing condition, the relative intensity of the back-to-back lobe compared to the side lobes should increase (starting from zero) as R departs from unity.

TDCSs were measured at $E = 25$ eV and $\varphi_1 = 0°$ for $R = 24$, 11.5, 4 and 2.57. These patterns are shown in polar form in figure 2, column 2. As with helium, the relative intensity of the back-to-back emission increases with increasing R; this trend is expected from the discussion above. The major difference between the helium and D_2 TDCSs, which is also evident in the Cartesian plots of figure 4, is that the 'three-lobe' structure almost disappears in D_2. This can be simply understood as a consequence of the more complicated form of $\sigma_{x,y}^{(3)C}$ (equations (8) and (9)), which involves four complex amplitudes with their various phases. More physically, the 'diffuse' structure of the D_2 TDCSs could be, at first sight, related to the averaging over molecular orientation. As discussed by Reddish and Feagin (1999), the negative value of the β parameter for ions (~ -0.7 at the present photon energy, see Kossmann *et al* (1989)) means that the Π component dominates over Σ. Consequently most of the molecules which are doubly ionized are likely to be oriented perpendicularly to the polarization axis and make an arbitrary angle with the present detection plane. If the TDCSs were to depend on this angle, the averaging at work in the present experiment could wash out their structure and be responsible for the observed diffuse shape. However such an explanation would be in contradiction with the assumption of Feagin's model, as discussed above, of an azimuthal symmetry about the ε_Π component, which we have estimated to be reasonable for the present kinematic conditions. More precisely, and returning to figure 4, the three-lobe structure which appears in helium but seems to disappear in D_2 occurs for low values of R, when the two electrons have their individual energies E_1 and $E_2 \leqslant 20$ eV, i.e. their wavelength larger than 5 au. In such conditions, as mentioned above, the azimuthal symmetry is expected to hold quite well. For these reasons, therefore, we believe that the main observed differences between helium and D_2 are more likely to be due to the intrinsic differences between the two targets than to averaging over molecular orientation. This conjecture might soon be tested by forthcoming experiments where the ions will be measured in coincidence with the two electrons, thus providing the TDCSs in the molecular frame.

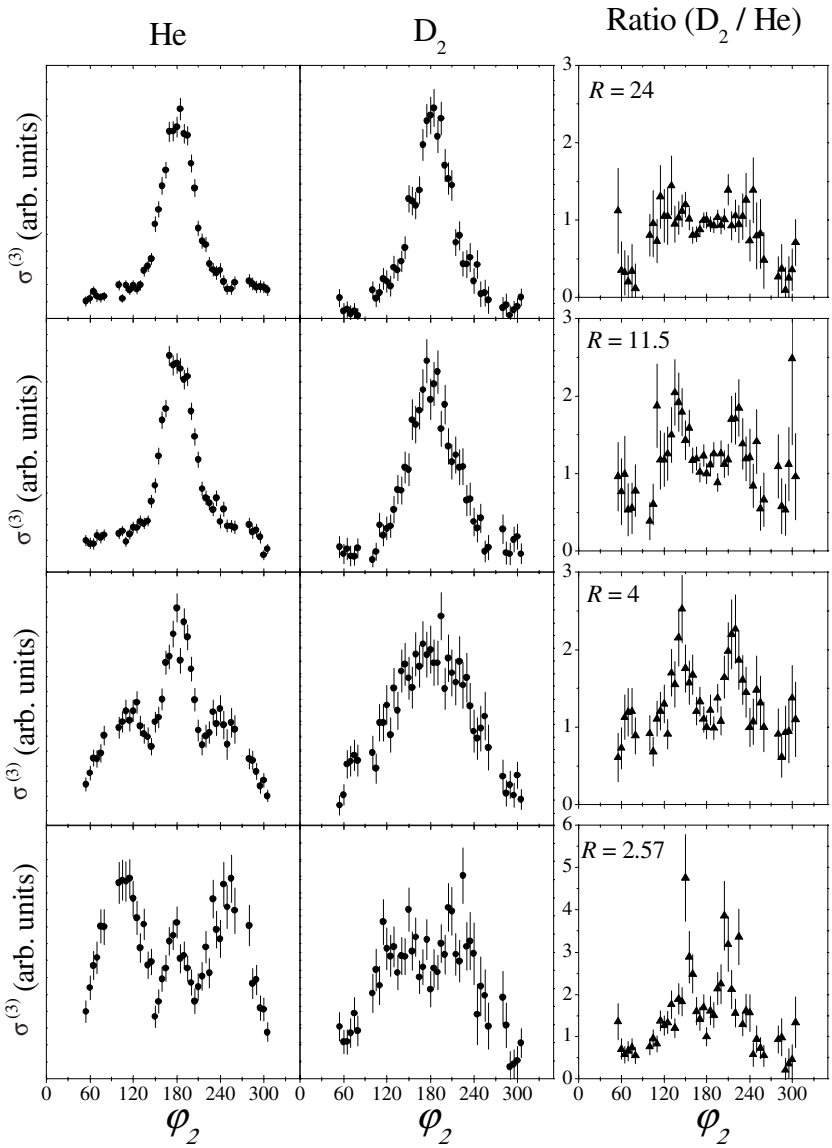

Figure 4. Cartesian plots of the He and D_2 TDCSs, together with their ratios. As the vertical scales for the TDCSs are arbitrary, the ratio plots are each normalized to unity at $\varphi_2 = 180°$.

Comparing the $R = 4$ plot with that presented in Collins *et al* (2001) (measured at $\phi_1 = 0°$), there is no indication of the back-to-back suppression suggested in the earlier data. As mentioned in the previous section, this could be due partly to the angular response normalization method adopted in Collins *et al* (2001). Additionally, as for helium, this discrepancy can be explained qualitatively as a consequence of S_1 not being unity ($S_1 = 0.9$). In this situation, $\sigma_y^{(3)}$ makes a significant contribution to $\sigma^{(3)}$ and since $\sigma_y^{(3)}$ has a different form in the two detection geometries, the overall TDCS plots can reasonably be expected to be different. If the 'molecular' term, $\frac{1}{15}[|a_\alpha|^2 + |a_\beta|^2 + 2\mathrm{Re}(a_\alpha a_\beta^*)\cos(\varphi_2 - \varphi_1)]$, is taken to be very small,

then $\sigma_y^{(3)C} \sim 0$ whilst $\sigma_y^{(3)P}$ has a two-lobe structure with a deep minimum for back-to-back emission (Collins *et al* 2001). Hence the contribution of $\sigma_y^{(3)C}$ may have a very small effect on the shape of the TDCS plot, while the effect of $\sigma_y^{(3)P}$ is to enhance the yield in the direction of side lobes. This behaviour is consistent with the observation in Collins *et al* (2001), but at odds with the explanation given. In Collins *et al* (2001), it was suggested that the 'suppression' (in the vicinity of $\theta_{12} = \pi$) could be due to interference caused by the two-centre nature of the target. The present evidence seems to suggest that the suppression is merely a consequence of the polarization state of the incident radiation, to which, as we have seen, TDCSs measured in the perpendicular geometry are particularly sensitive.

To highlight the differences between the two targets, the ratio, $\sigma_{ratio}^{(3)C} = \sigma_{D_2}^{(3)C}/\sigma_{He}^{(3)C}$, has been determined as a function of φ_2 for each energy-sharing condition. Since the measured TDCSs are non-absolute, we have normalized the $\sigma_{ratio}^{(3)C}$ values to unity at $\varphi_2 = 180°$ for each R and the resulting plots are shown in figure 4. Each plot, as it should, has good reflection symmetry about $\varphi_2 = 180°$ and in general $\sigma_{ratio}^{(3)C}$ increases as φ_2 is varied from $\sim$60° to 150° and decreases as φ_2 is varied from $\sim$150° to 180°. The evolution of $\sigma_{ratio}^{(3)C}$ with R is striking, with the peak at $\varphi_2 \approx 150°$ becoming 'sharper' and moving closer to 180° as R is decreased. Note that this trend is consistent with the plot of $\sigma_{ratio}^{(3)P}$ presented in Wightman *et al* (1998), for $E = 20$ eV and $R = 1$, that consists of a single peak at $\phi_2 = 180°$; this was later explained as a solid angle effect due to the differences in the three-dimensional nodal structure of the TDCS (Feagin 1998, Reddish and Feagin 1999). If one makes the assumption that the mutual angle dependences of a_Σ^g, a_Π^g and of a_Σ^u, a_Π^u are similar, so that there effectively exists one overall gerade amplitude (a_g) and one overall ungerade amplitude (a_u), a number of deductions can be made from the $\sigma_{ratio}^{(3)}$ plots. Firstly in the $R = 2.57$ plot at mutual angles around 90°, the *gerade* amplitude can reasonably be assumed to be dominant and the positive gradient in this region implies that a_g is narrower in D_2 than in He. (Had the ratio been essentially 'flat' in this region, a_g in the two targets would have similar widths.) The present study, therefore, has similar findings to Wightman *et al* (1998), who fitted their He and D_2 TDCSs (measured at $E = 20$ eV, $R = 1$) using Gaussian functions and obtained the half-widths of $77° \pm 3°$ and $91° \pm 3°$ for D_2 and He, respectively. Similar results were also obtained by Collins *et al* (2001) ($E = 25$ eV, $R = 4$) using their $\phi_1 = 90°$ TDCSs. Secondly, in the $R = 24$ plot, the *ungerade* amplitude dominates at $\varphi_2 \sim 180°$ and the broad, near-zero gradient in this angular region suggests that the shapes of a_u in both targets are not too dissimilar. The peak at $\varphi_2 \approx 150°$ can then be understood as simply due to the differences in the mutual angle dependences of the gerade and ungerade amplitudes. These noteworthy, if oversimplified, conclusions, which fail to separate the role of the individual Σ and Π amplitudes, are indicative of interesting unexplored physics and clear differences in the PDI dynamics of D_2 and He. A further important feature of the measured $\sigma_{ratio}^{(3)C}$ is that it eliminates any potential θ_{12}-dependent systematic errors, as the D_2 and He TDCSs for each R were obtained using virtually identical spectrometer conditions. Thus this ratio constitutes a sensitive and highly reliable test for future calculations.

4. Conclusions

(γ, 2e) angular distributions in D_2 have been measured for a range of electron energy asymmetries and compared with corresponding helium TDCSs at the same fixed excess energy of 25 eV. For all kinematic conditions studied, very good agreement has been found between the measured helium TDCSs and those calculated using the H$\Re$M-SOW method. Concerning D_2, our previous preliminary measurements (Collins *et al* 2001) suggested that

a two-centre interference effect, going beyond Feagin's helium-like model, could occur. The present work shows that the slight back-to-back suppression reported there is most likely due to polarization rather than interference effects. Although the Feagin model provides some useful insights into the main features of the TDCSs, the present D_2 results strongly appeal for an extension to molecules of the theoretical methods (CCC, TDCC, ECS and H$\Re$M-SOW) recently developed for helium.

Acknowledgments

This work was funded by EPSRC and the EU large-scale facilities fund at the LURE laboratory (Orsay, France). DPS and SAC thank EPSRC for their PDRA and studentship positions, respectively. The H$\Re$M-SOW calculations were performed on the NEC-SX5 of the CNRS computer centre IDRIS (Orsay, France).

References

Baertschy M, Rescigno T N, Isaacs W A, Li X and McCurdy C W 2001 *Phys. Rev.* A **63** 022712
Berakdar J and Klar H 1992 *Phys. Rev. Lett.* **69** 1175
Bray I and Stelbovics A T 1992 *Phys. Rev.* A **46** 6995
Briggs J S and Schmidt V 2000 *J. Phys. B: At. Mol. Opt. Phys.* **33** R1
Chandra N and Sen S 1999 *Eur. Phys. J.* D **6** 457
Colgan J and Pindzola M S 2002 *Phys. Rev.* A **65** 032729
Colgan J, Pindzola M S and Robicheaux F 2001 *J. Phys. B: At. Mol. Opt. Phys.* **34** L457
Collins S A *et al* 2002 *Phys. Rev.* A **65** 052717
Collins S A, Huetz A, Reddish T J, Seccombe D P and Soejima K 2001 *Phys. Rev.* A **64** 062706
Dawson C, Cvejanović S, Seccombe D P, Reddish T J, Maulbetsch F, Huetz A, Mazeau J and Kheifets A S 2001 *J. Phys. B: At. Mol. Opt. Phys.* **34** L525
Dörner R *et al* 1998 *Phys. Rev. Lett.* **81** 5776
Dujardin G, Besnard M J, Hellner L and Malinovitch Y 1987 *Phys. Rev.* A **35** 5012
Feagin J M 1998 *J. Phys. B: At. Mol. Opt. Phys.* **31** L729
Huetz A, Andric L, Selles P, Jean A, Lablanquie P and Mazeau J 1995 *19th Int. Conf. on Physics of Electronic and Atomic Collisions* ed L J Dude, J B A Mitchell, J W McConkey and C E Brion (New York: American Institute of Physics) p 139
Huetz A and Mazeau J 2000 *Phys. Rev. Lett.* **85** 530
Huetz A, Selles P, Waymel D and Mazeau J 1991 *J. Phys. B: At. Mol. Opt. Phys.* **24** 1917
Joy H W and Parr R G 1958 *J. Chem. Phys.* **28** 448
Kheifets A S and Bray I 1998 *J. Phys. B: At. Mol. Opt. Phys.* **31** L447
Kossmann H, Schwarzkopf O, Kämmerling B and Schmidt V 1989 *Phys. Rev. Lett.* **63** 2040
Lablanquie P, Mazeau J, Andrić L, Selles P and Huetz A 1995 *Phys. Rev. Lett.* **74** 2192
Malegat L, Selles P and Kazansky A K 2000 *Phys. Rev. Lett.* **85** 4450
Maulbetsch F and Briggs J S 1995 *J. Phys. B: At. Mol. Opt. Phys.* **28** 551
Mazeau J, Andrić L, Jean A, Lablanquie P, Selles P and Huetz A 1996 *Atomic and Molecular Photoionization* ed A Yagishita and T Sasaki (Tokyo: Universal Academy) pp 31–8
Mazeau J, Lablanquie P, Selles P, Malegat L and Huetz A 1997 *J. Phys. B: At. Mol. Opt. Phys.* **30** L293
Pindzola M S and Robicheaux F J 2000 *Phys. Rev.* A **61** 052707
Posthumus J H, Plumridge J, Taday P F, Sanderson J H, Langley A J, Codling K and Bryan W A 1999 *J. Phys. B: At. Mol. Opt. Phys.* **32** L93
Reddish T J and Feagin J M 1999 *J. Phys. B: At. Mol. Opt. Phys.* **32** 2473
Reddish T J, Richmond G, Bagley G W, Wightman J P and Cvejanović S 1997a *Rev. Sci. Instrum.* **68** 2685
Reddish T J, Wightman J P, MacDonald M A and Cvejanović S 1997b *Phys. Rev. Lett.* **79** 2438
Rescigno T N, Baertschy M, Isaacs W A and McCurdy C W 1999 *Science* **286** 2474
Scherer N, Lörch H and Schmidt V 1998 *J. Phys. B: At. Mol. Opt. Phys.* **31** L817
Schwarzkopf O, Krässig B, Elmiger J and Schmidt V 1993 *Phys. Rev. Lett.* **70** 3008
Schwarzkopf O, Krässig B, Schmidt V, Maulbetsch F and Briggs J S 1994 *J. Phys. B: At. Mol. Opt. Phys.* **27** L347
Schwarzkopf O and Schmidt V 1995 *J. Phys. B: At. Mol. Opt. Phys.* **28** 2847

Selles P, Malegat L and Kazansky A K 2002 *Phys. Rev.* A **65** 032711
Sen S and Chandra N 2000 *Phys. Rev.* A **62** 052702
Staudte A, Cocke C L, Prior M H, Belkacem A, Ray C, Chong H W, Glover T E, Schoenlein R W and Saalmann U 2002 *Phys. Rev.* A **65** 020703(R)
Trump C, Rottke H and Sander W 1999 *Phys. Rev.* A **60** 3924
Walter M and Briggs J S 1999 *J. Phys. B: At. Mol. Opt. Phys.* **32** 2487
Walter M and Briggs J S 2000 *Phys. Rev. Lett.* **85** 1630
Walter M, Briggs J S and Feagin J M 2000 *J. Phys. B: At. Mol. Opt. Phys.* **33** 2907
Wehlitz R, Langer B, Berrah N, Whitfield S B, Viefhaus J and Becker U 1993 *J. Phys. B: At. Mol. Opt. Phys.* **26** L783
Wightman J P, Cvejanović S and Reddish T J 1998 *J. Phys. B: At. Mol. Opt. Phys.* **31** 1753